Torque Ripple Reduction and Flux-Droop Minimization of DTC With Improved Interleaving CSFTC of IM Fed by Three-Level NPC Inverter

SAMER SALEH HAKAMI, (Student Member, IEEE),
IBRAHIM MOHD ALSOFYANI, (Member, IEEE), AND
KYO-BEUM LEE, (Senior Member, IEEE)
Department of Electrical and Computer Engineering, Ajou University, Suwon 16499, South Korea

Corresponding author: Kyo-Beum Lee (kyl@ajou.ac.kr)

ABSTRACT Direct torque control (DTC) is known for its fast control in AC motor drives due to its simple control structure that directly controls the torque without the need for modulation blocks or frame transformations. However, when used in induction motor (IM) drives it has three main drawbacks: large torque ripples, variable switching frequency, and sector flux-droop at the low-speed region due to the employment of the torque hysteresis controller (THC). Torque ripple minimization can be achieved in DTC drives by replacing the originally proposed two-level inverter with a three-level neutral-point clamped (3L-NPC) inverter. Nevertheless, the switching frequency remains variable and low, which produces an elevated torque ripple and asymmetrical switching signals for the inverter. In addition, sector flux-droop resulting from driving the IM at the low-speed region produces a high current distortion that consequently eliminates the robustness of DTC. To alleviate these problems, an interleaving constant switching frequency torque controller-based DTC (CSFTC-DTC) was implemented. It improves the operation of the IM at the low-speed region by increasing the duty-cycle of the applied active voltage vector and reducing the duration of the applied zero vectors. Although the conventional CSFTC-DTC regulates the stator flux of the IM at the low-speed region and minimizes the total harmonic distortion (THD) of the stator current, it produces a high torque ripple—one of the main disadvantages of classical DTC. In this paper, an interleaving CSFTC-DTC is proposed to subdivide the duty cycle of the applied vectors of the 3L-NPC inverter to limit the influence of the large duty-cycle of the applied vectors on flux-regulation and torque ripples. The simulation and experimental results presented validate the effectiveness of the proposed method over the conventional method.

INDEX TERMS Constant switching frequency torque controller, direct torque control, induction motor, three-level neutral-point clamped inverter.

NOMENCLATURE
LISTOFACRONYMS

DTC	Direct torque control.
FOC	Field oriented control.
MPC	Model predictive control.
SVM	Space vector modulation.
DR	Duty ratio.
PI	Proportional integral.
IM	Induction Motor.

PMSM	Permanent magnet synchronous motor.
THC	Torque hysteresis controller.
MLI	Multilevel inverter.
NPC	Neutral point clamped.
CSFTC	Constant switching frequency torque controller.
THD	Total harmonics distortion.
DC	Direct current.
FFT	Fast Fourier transform.

LISTOFSYMBOLS

P	Positive.
O	Null.
N	Negative.

The associate editor coordinating the review of this manuscript and approving it for publication was Xiaodong Sun.

Sx	Inverter switch.
Dx	Inverter diode.
x	Phase a,b,c.
i_a	Phase (a) current.
i_b	Phase (b) current.
i_c	Phase (c) current.
$\boldsymbol{v_s}$	Stator voltage vector.
$\boldsymbol{i_s}$	Stator current vector.
$\boldsymbol{i_r}$	Rotor current vector.
$\boldsymbol{\lambda_s}$	Stator flux vectors.
$\boldsymbol{\lambda_r}$	Rotor flux vectors.
R_s	Stator resistor.
R_r	Rotor resistor.
L_s	Stator inductor.
L_m	Mutual inductor.
L_r	Rotor inductor.
ω_r	Rotor electric angular motor speed.
p	Number of pole pair.
Im	Imaginary.
α, β	Stationary reference frame axes.
T_e	Electromagnetic torque.
$T_{e\,ripple}$	Torque ripple.
$*$	Denotes reference value.
T_c	Output of torque PI controller.
$C_{upper3},$	Interleaving upper carriers for medium and high.
C_{upper4}	speed operation in forward direction.
$C_{upper1},$	Interleaving upper carriers for low speed.
C_{upper2}	operation in forward direction.
$C_{lower3},$	Interleaving lower carriers for medium and high.
C_{lower4}	speed operation in reverse direction.
$C_{lower1},$	Interleaving lower carriers for low speed.
C_{lower2}	operation in reverse direction.
C_{p-p}	Peak-to-peak value of interleaving carriers

I. INTRODUCTION

Classical direct torque control (DTC) has been the focus of numerous studies during the past four decades for its excellent control features compared to field orientated control (FOC) [1], [2]. The DTC provides fast control of AC motors because the torque and flux are controlled directly without any modulation techniques or frame transformations [3]. Despite its fast dynamic response, there are some issues associated with the use of a torque hysteresis controller-based DTC (THC-DTC), such as high torque ripples and variable switching frequency. Moreover, there is a flux-droop at the low-speed region of induction motor (IM) drives [4], [5].

As reported in the literature, there have been various endeavors to address the deficiencies in THC-DTC drives. Introducing space vector modulation to classical DTC (DTC-SVM) is the most common strategy used to improve the performance of THC-DTC [6]. However, it is difficult to estimate the appropriate reference voltage in the SVM technique [7]. Additional control techniques, such as a proportional-integral (PI) [8], dead-beat control [9], sliding mode controller [6], extended Kalman filter (EKF) [10],

model reference adaptive systems (MRAS) [11], internal model control [12], state feedback control [13] and artificial neural networks (ANN) [14] for torque and flux regulation are required.

The second alternative control strategy is model predictive control (MPC) that requires a predefined cost function to predict output states, obtain state variables, and execute control object optimization [15]–[19]. Another approach for the improvement of DTC is the control of the duty-ratio of the applied voltage vectors (DR-DTC) [20]–[23]. In DR-DTC, the duty-ratios of the applied voltage vectors are adjusted to minimize torque and flux ripples. However, the switching frequency is not fixed.

In addition to the advantages of these sophisticated algorithms used to improve the performance of classical DTC, torque and flux ripples can be minimized by employing multilevel inverters (MLIs), as the output voltage of MLIs is synthesized with a higher number of discrete levels compared to two-level inverters. Among MLIs topologies used in DTC drives [24]–[27], a three-level neutral-point clamped (3L-NPC) inverter is the most prominent. In DTC fed by a 3L-NPC inverter, the selection of applied voltage vectors is expanded, thus different speeds of stator flux linkage can be achieved to have predominant control of torque and flux.

Recently, researchers have focused on fixing the switching frequency of classical DTC by replacing the THC with a constant switching frequency torque controller (CSFTC). The CSFTC, composed of triangular carriers and a PI controller, is able to reduce variability in the switching frequency and minimize torque ripples compared to THC-DTC. Therefore, it is a robust strategy to tackle the limitations of classical DTC. Some studies of CSFTC have also examined MLIs with DTC of IMs [27]–[30] and permanent magnet synchronous machines (PMSMs) [31]. Among these studies, the authors in [25], [30] proposed a 3L-NPC inverter for CSFTC-DTC to further reduce both flux and torque ripples and to obtain smoother responses. Although good performance, such as fixed switching frequency and minimized torque and flux ripples was achieved in most of these previous studies, none have improved the critical low-speed operation of IMs that causes stator flux drops due to the domination of the stator resistor and the selection of a zero voltage vector [4], [5]. In [32], [33] the sector flux-droop has been corrected by increasing the duty cycle of the applied active vector using interleaving carriers. Nevertheless, this technique results in large flux and torque ripples, which are comparable to those produced by classical THC-DTC.

This paper proposes an improved interleaving CSFTC based 3L-DTC algorithm for IM drives with reduced torque ripple. Unlike the method in [32], the proposed method is used to reduce torque ripples by shortening the duty ratio of the applied active-voltage vectors and reducing the duration of zero-voltage vectors while maintaining the merits of the conventional interleaving CSFTC for the 3L-NPC inverter. In addition to torque ripple reduction, the proposed algorithm minimizes the flux-droop at the low-speed region,
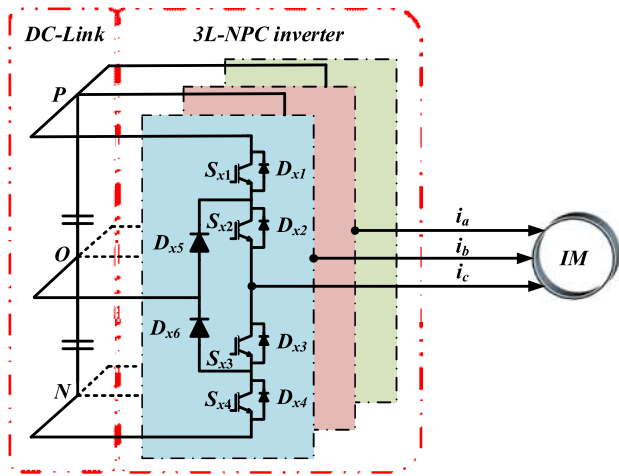
FIGURE 1. Circuit topology of 3L-NPC inverter.

thus leading to a significant improvement in the performance of the stator current waveform. The effectiveness of the proposed algorithm is validated through simulation and experimental results.

II. SYSTEM MODELLING

A. IM IN STATIONARY REFERENCE FRAME

The mathematical modelling of the induction machine (IM) is expressed in terms of space vectors as given below:

$$v_s = R_s i_s + \frac{d\lambda_s}{dt} \tag{1}$$

$$0 = R_r i_r - j\omega_r \lambda_r + \frac{d\lambda_r}{dt} \tag{2}$$

$$\lambda_s = L_s i_s + L_m i_r \tag{3}$$

$$\lambda_r = L_r i_r + L_m i_s \tag{4}$$

$$T_e = \frac{3}{2} p.Im(\lambda_s \cdot i_s) \tag{5}$$

B. 3L-NPC INVERTER

The three-level neutral-point clamped (3L-NPC) inverter is the most common among MLI topologies in DTC drives. The basic structure of 3L-NPC inverter is illustrated in Fig. 1. The space vector diagram and switching states of 3L-NPC inverter are shown in Fig. 2.

It can be seen that 27 switching states represent the connection of the stator to the DC power supply. In Fig. 2, "-1," "0," and "1," denotes a connection to a negative DC rail, neutral point, and positive DC rail, respectively. There are 19 distinct voltage vectors: large ($V_1 - V_6$), medium ($V_7 - V_{12}$), small ($V_{13} - V_{18}$), and zero (V_0). The switching states are of P-types or N-types as shown in Fig. 2. P-type means the phases are connected to the positive DC rail and the neutral point. While N-type switching state means that phases are connected to the neutral point and the negative DC rail. P-type and N-type switching states mostly causes neutral point voltage deviation. P-type states increase the lower DC-link capacitor voltage, whereas the N-type state decreases the lower DC-link capacitor voltage in motoring mode.
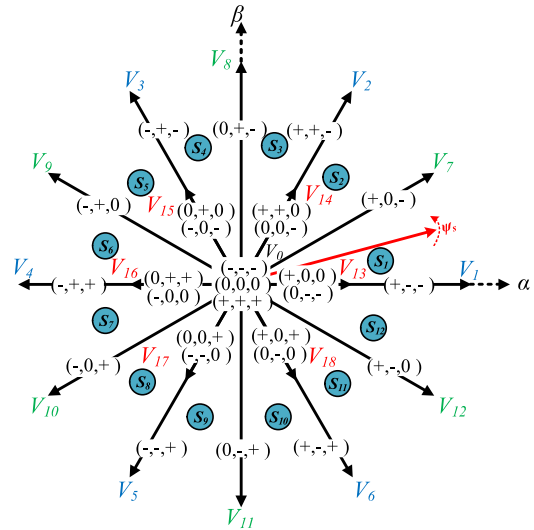

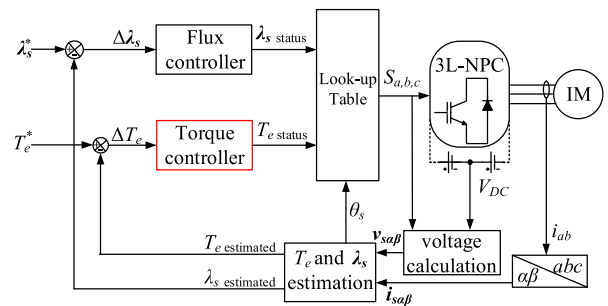**FIGURE 2.** Space vector diagram of 3L-NPC inverter.

FIGURE 3. Structure of DTC fed by 3L-NPC inverter for IM drives.
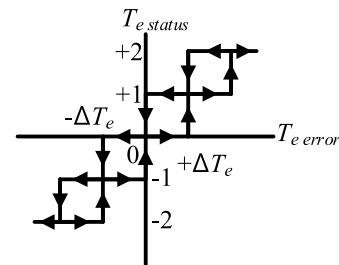

FIGURE 4. Five-level THC.

III. DTC FOR 3L-NPC INVERTER

Fig. 3 shows the complete structure of DTC for controlling the IM fed by 3L-NPC inverter. The main idea of this topology is applying hysteresis torque and flux controllers for controlling both stator flux λ_s and electromagnetic torque T_e. The design of the torque hysteresis controller (THC) is shown in Fig. 4. With the output of the THC, the inverter switching states can be selected from a predefined look-up table (see Table 1). This look-up table has 12 sectors to increase the degree of freedom of voltage vectors selection. The $T_{e\,status}$ and $\lambda_{s\,status}$ are responsible for controlling both the T_e and λ_s according to the commanded values and speed of the IM.

TABLE 1. Lookup table for DTC fed by 3L-NPC inverter.

$\lambda_{s\ status}$	$T_{e\ status}$	$S_{ector\ 1}$	$S_{ector\ 2}$	$S_{ector\ 3}$	$S_{ector\ 4}$	$S_{ector\ 5}$	$S_{ector\ 6}$	$S_{ector\ 7}$	$S_{ector\ 8}$	$S_{ector\ 9}$	$S_{ector\ 10}$	$S_{ector\ 11}$	$S_{ector\ 12}$
	+2	V_3	V_9	V_4	V_{10}	V_5	V_{11}	V_6	V_{12}	V_1	V_7	V_2	V_8
	+1	V_{15}	V_{15}	V_{16}	V_{16}	V_{17}	V_{17}	V_{18}	V_{18}	V_{13}	V_{13}	V_{14}	V_{14}
1	0	V_0	V_0	V_0	V_0	V_0	V_0	V_0	V_0	V_0	V_0	V_0	V_0
	-1	V_{18}	V_{18}	V_{13}	V_{13}	V_{14}	V_{14}	V_{15}	V_{15}	V_{16}	V_{16}	V_{17}	V_{17}
	-2	V_{11}	V_6	V_{12}	V_1	V_7	V_2	V_8	V_3	V_9	V_4	V_{10}	V_5
	+2	V_2	V_8	V_3	V_9	V_4	V_{10}	V_5	V_{11}	V_6	V_{12}	V_1	V_7
	+1	V_{14}	V_{14}	V_{15}	V_{15}	V_{16}	V_{16}	V_{17}	V_{17}	V_{18}	V_{18}	V_{13}	V_{13}
0	0	V_0	V_0	V_0	V_0	V_0	V_0	V_0	V_0	V_0	V_0	V_0	V_0
	-1	V_{13}	V_{13}	V_{14}	V_{14}	V_{15}	V_{15}	V_{16}	V_{16}	V_{17}	V_{17}	V_{18}	V_{18}
	-2	V_{12}	V_1	V_7	V_2	V_8	V_3	V_9	V_4	V_{10}	V_5	V_{11}	V_6

A. TORQUE AND FLUX ESTIMATION

It is worthy to note that all calculations are carried out in the stationary reference frame for estimating the λ_s and T_e from the α-β components of stator current $\mathbf{i}_s$ and stator voltage $\mathbf{v}_s$ as follow:

$$\lambda_{s\alpha} = \int (v_{s\alpha} - R_s i_{s\alpha})dt \tag{6}$$

$$\lambda_{s\beta} = \int (v_{s\beta} - R_s i_{s\beta})dt \tag{7}$$

$$|\lambda_s| = \sqrt{\lambda_{s\alpha}^2 + \lambda_{s\beta}^2} \tag{8}$$

$$T_e = \frac{3p}{2}\left(\lambda_{s\alpha} i_{s\beta} - \lambda_{s\beta} i_{s\alpha}\right) \tag{9}$$

Based on the switching states $S_{a,b,c}$ determined from the look-up table, the voltage vectors, $v_{s\alpha}$ and $v_{s\beta}$ are estimated as given by:

$$v_{s\alpha} = \frac{1}{3}V_{DC}(2S_a - S_b - S_c) \tag{10}$$

$$v_{s\beta} = \frac{1}{\sqrt{3}}V_{DC}(S_b - S_c) \tag{11}$$

B. TORQUE HYSTERESIS CONTROLLER

One of the main components of classical DTC is of the THC. The design of the THC depends on the output voltage level of the inverter used because the output status of the THC will select the appropriate voltage vectors of the inverter that need to be used to satisfy the DTC operation. In the literature, improvements in the design of a five-level THC (Fig. 4) allow more voltage vectors to be selected for a 3L-NPC depending on the speed region of the motor. The main advantages of using a five-level THC is that the torque ripple is reduced and the degree of freedom is increased for selecting the voltage vectors of the 3L-NPC inverter is limited in this topology. All voltage vector types of a 3L-NPC inverter can be used to drive the IM in a DTC system.

However, it does not solve the problem of the variable switching frequency of classical DTC. Moreover, it has poor performance in low-speed region of the IM drives due to the unregulated λ_s. The output rules for the five-level THC are

expressed as:

$$T_{e\ status} = \begin{cases} +2 & for\ T_{e\ error} \geq \Delta T_e \\ +1 & for\ \Delta T_e/2 < T_{e\ error} < \Delta T_e \\ +0 & for\ 0 < T_{e\ error} < \Delta T_e/2 \\ -0 & for\ -\Delta T_e/2 < T_{e\ error} < 0 \\ -1 & for\ -\Delta T_e < T_{e\ error} < -\Delta T_e/2 \\ -2 & for\ T_{e\ error} \leq -\Delta T_e \end{cases} \tag{12}$$

where $T_{e\ status}$ is the torque status, which can be either of the following states $+2$, $+1$, $+0$, -0, -1, -2. By using these rules, the IM will operate smoothly in a wide speed range. A positive torque status indicates that the operation is in the forward direction, whereas a negative torque status indicates that the motor is rotating in the reverse direction.

IV. CONSTANT SWITCHING FREQUENCY TORQUE CONTROLLER FOR 3L-NPC INVERTER

The CSFTC has been used to mitigate the problems associated with the classical THC-DTC. It helps the switching frequency to remain constant and reduces torque ripples. However, the classical CSFTC suffers from sector flux-droop at the low-speed region due to a small duty cycle of the applied small active vector causing high distortions in current waveforms. An interleaving CSFTC was introduced to improve the performance of the IM drive at the low-speed region by minimizing the drop of λ_s. The complete structure of the interleaving CSFTC is shown in Fig. 5. It consists of five-level of interleaving carriers which is designed based on the five-level THC. This controller needs a PI controller to minimize the steady-state error and reduce the torque ripples. The output of the PI controller is T_c signal. The main function of the comparators is to compare the T_c with the 5-level interleaving carriers. The output status of this comparison will be sent to the look-up table based of the operation of the IM.

The performance of the CFTC is affected by the proportional gain (k_p) and integral gain (k_i) of the PI controller. The PI gains of the interleaving CSFTC are designed according to [32] by considering the full amplitude of the triangular carrier, as the PI output, T_c should not exceed the maximum value of triangular carrier (C_{p-p}). In this paper, the k_p and k_i of the interleaving CSFTC are set to 4.326 and 158.02 respectively.
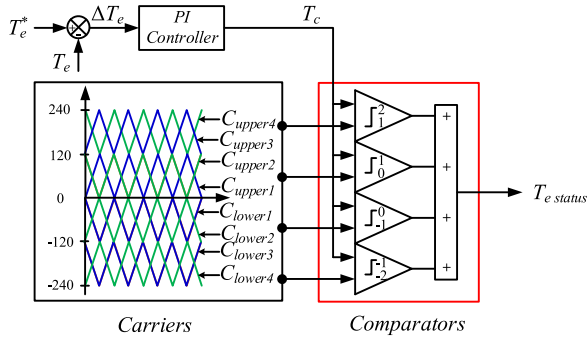
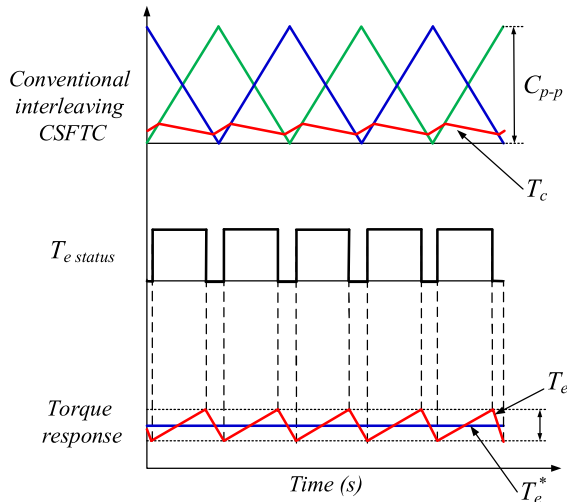**FIGURE 5.** Complete structure of interleaving CSFTC.

FIGURE 6. Operational principle of conventional interleaving CSFTC [32].

A. CONVENTIONAL INTERLEAVING CSFTC

The conventional interleaving CSFTC has been proposed to improve the low-speed operation of the IM drives fed by two-level inverter where the $|\lambda_s|$ droops due to the high domination of the R_s [32]. The main advantage of using the conventional interleaving CSFTC is to keep the switching frequency constant and regulate the λ_s. However, this technique produces high torque and flux ripples. To understand the problem of the conventional interleaving CSFTC, the operational principle is illustrated as shown in Fig. 6. As shown from the mechanism of this controller that the duty cycle of the zero-voltage vector is shortened to limit the effect of the domination of the R_s during the operation of the IM drives, particularly in the low-speed region. As a result, the duty cycle of the applied active vectors will be large which causes high torque and flux ripples that it is not desirable for advanced motor drives applications. The output rules for the conventional interleaving CSFTC are shown in Table 2.

B. PROPOSED INTERLEAVING CSFTC

Fig. 7 shows the operational principle of the proposed interleaving CSFTC, which has attained the merits of a conventional interleaving CSFTC and has improved the operation of the IM at the low-speed region by regulating the λ_s, resulting in less current distortion as compared to the classical

TABLE 2. Conventional interleaving CSFTC rules.

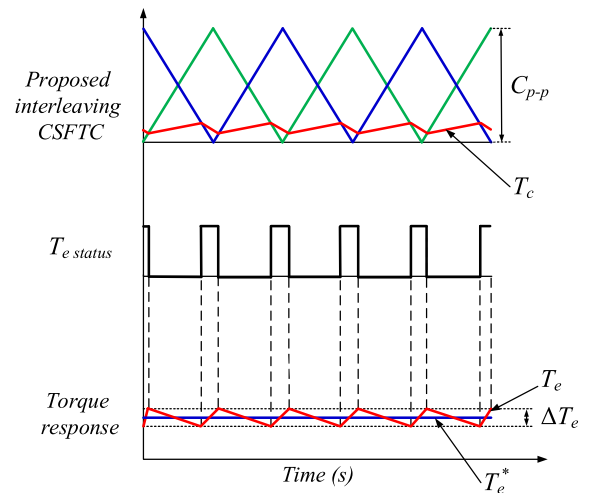| Conditions	Output
$(C_{upper1} < T_c \ \&\& \ T_c < C_{upper2})$ $\parallel$ $(C_{upper2} < T_c \ \&\& \ T_c < C_{upper1})$	+2
$(C_{upper3} < T_c \ \&\& \ T_c < C_{upper4})$ $\parallel$ $(C_{upper4} < T_c \ \&\& \ T_c < C_{upper3})$	+1
$(0 < T_c \ \&\& \ T_c < C_{upper1})$ $\parallel$ $(0 < T_c \ \&\& \ T_c < C_{upper2})$	-0
$(C_{lower1} < T_c \ \&\& \ T_c < 0)$ $\parallel$ $(C_{lower2} < T_c \ \&\& \ T_c < 0)$	-0
$(C_{lower3} < T_c \ \&\& \ T_c < C_{lower4})$ $\parallel$ $(C_{lower4} < T_c \ \&\& \ T_c < C_{lower3})$	-1
$(C_{lower1} < T_c \ \&\& \ T_c < C_{lower2})$ $\parallel$ $(C_{lower2} < T_c \ \&\& \ T_c < C_{lower1})$	-2

FIGURE 7. Operational principle of proposed interleaving CSFTC.

TABLE 3. Proposed interleaving CSFTC rules.

Conditions	Output
$(C_{upper3} < T_c \ \&\& \ T_c < C_{upper4})$ $\parallel$ $(C_{upper4} < T_c \ \&\& \ T_c < C_{upper3})$	+2
$(C_{upper1} < T_c \ \&\& \ T_c < C_{upper2})$ $\parallel$ $(C_{upper2} < T_c \ \&\& \ T_c < C_{upper1})$	+1
$(0 < T_c \ \&\& \ T_c < C_{upper1})$ $\parallel$ $(0 < T_c \ \&\& \ T_c < C_{upper2})$	+0
$(C_{lower1} < T_c \ \&\& \ T_c < 0)$ $\parallel$ $(C_{lower2} < T_c \ \&\& \ T_c < 0)$	-0
$(C_{lower1} < T_c \ \&\& \ T_c < C_{lower2})$ $\parallel$ $(C_{lower2} < T_c \ \&\& \ T_c < C_{lower1})$	-1
$(C_{lower3} < T_c \ \&\& \ T_c < C_{lower4})$ $\parallel$ $(C_{lower4} < T_c \ \&\& \ T_c < C_{lower3})$	-2

THC based DTC. The proposed interleaving CSFTC is able to prevent high torque and flux ripple, especially in the low-speed region. Additionally, the duty cycle in the proposed CSFTC is shorter than that in the conventional interleaving CSFTC [32], which can significantly minimize the drop of the $|\lambda_s|$ in the low-speed region. In addition, the proposed interleaving CSFTC has a further reduction in torque ripple
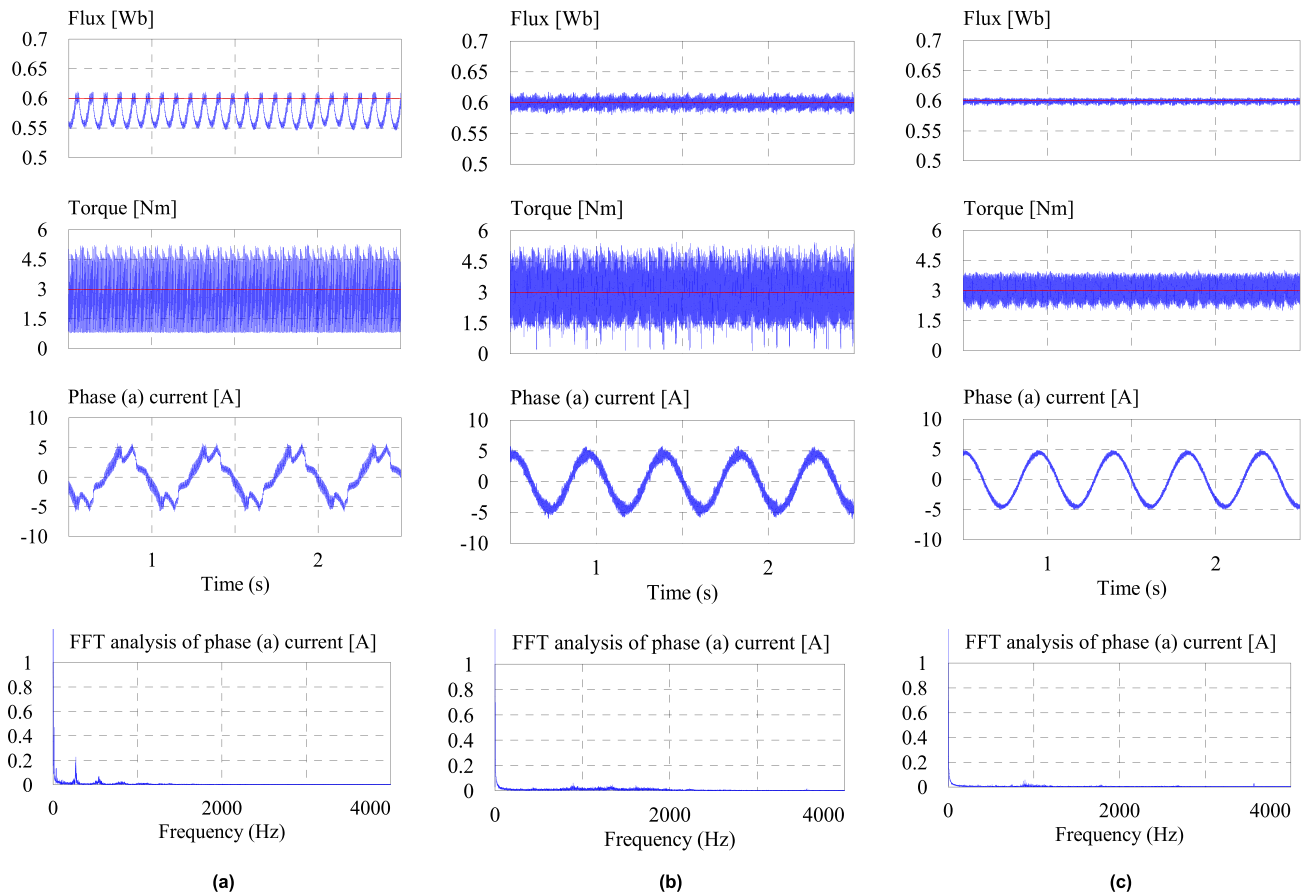
FIGURE 8. Simulation results of steady-state response of the IM at 50 r/min, 3 Nm: (a) five-level THC; (b) conventional interleaving CSFTC; (c) proposed interleaving CSFTC; from top to bottom: flux response, torque response, stator current, and FFT analysis of the stator current (reference values: red; estimated: blue).

as it reduces the duration of the small, medium, or large active vectors that are applied to increase the torque. Table 3 shows the proposed interleaving CSFTC rules.

The proposed algorithm is able to overcome the limitations of the conventional interleaving CSFTC based DTC, thus resulting in better IM drives performance for a wide speed range.

V. SIMULATION RESULTS

The effectiveness of the proposed interleaving CSFTC is investigated in this section using PSIM software. The performance of the proposed method is investigated and then compared with that of the five-level THC-DTC and conventional interleaving CSFTC methods proposed in [32]. Among the three methods, the proposed interleaving CSFTC has the lowest torque and flux ripples. Moreover, it retains the merits of the conventional interleaving CSFTC in improving the low-speed operation of the IM drives by minimizing the drop of the $|\lambda_s|$. In addition, the proposed interleaving CSFTC has excellent control in medium and high-speed operation of the IM drives fed by 3L-NPC inverter in reducing the torque ripples compared to the five-level THC-DTC and conventional interleaving CSFTC methods. Therefore, the steady-state performance of the proposed interleaving CSFTC method is

TABLE 4. IM parameters.

Parameter	Value	Parameter	Value
Rated power	3.7 kW	Stator resistance	0.934 Ω
Rated current	8.28 A	Rotor resistance	1.225 Ω
Rated speed	1750 r/min	Stator inductance	146.213 mH
Rated Torque	20.36 Nm	Rotor inductance	146.213 mH
Rated flux	0.6 Wb	Mutual inductance	139.516 mH
Pole pairs	2	Total leakage factor	1.91049

compared with that of the five-level THC-DTC and conventional interleaving CSFTC methods in various speed regions. In order to compare the performance of the above mentioned DTC methods in a similar condition, the motor and control system parameters in all the simulations are adjusted to the same as those used in [32]. These parameters are tabulated in Table 4. In order to achieve lower torque ripples for five-level THC-DTC, the band size of THC is set to be 10% of rated torque (i.e, $\Delta T_e/2 = 2$ Nm), whereas the stator flux band is 0.0015 Wb. The simulation sampling time is set to 70 μs.

A. LOW-SPEED OPERATION

Fig. 8 shows the simulation results for the five-level THC, conventional interleaving CSFTC, and proposed interleaving CSFTC based DTC methods at 50 r/min. It is evident that the flux-droop is significant in the five-level THC that results
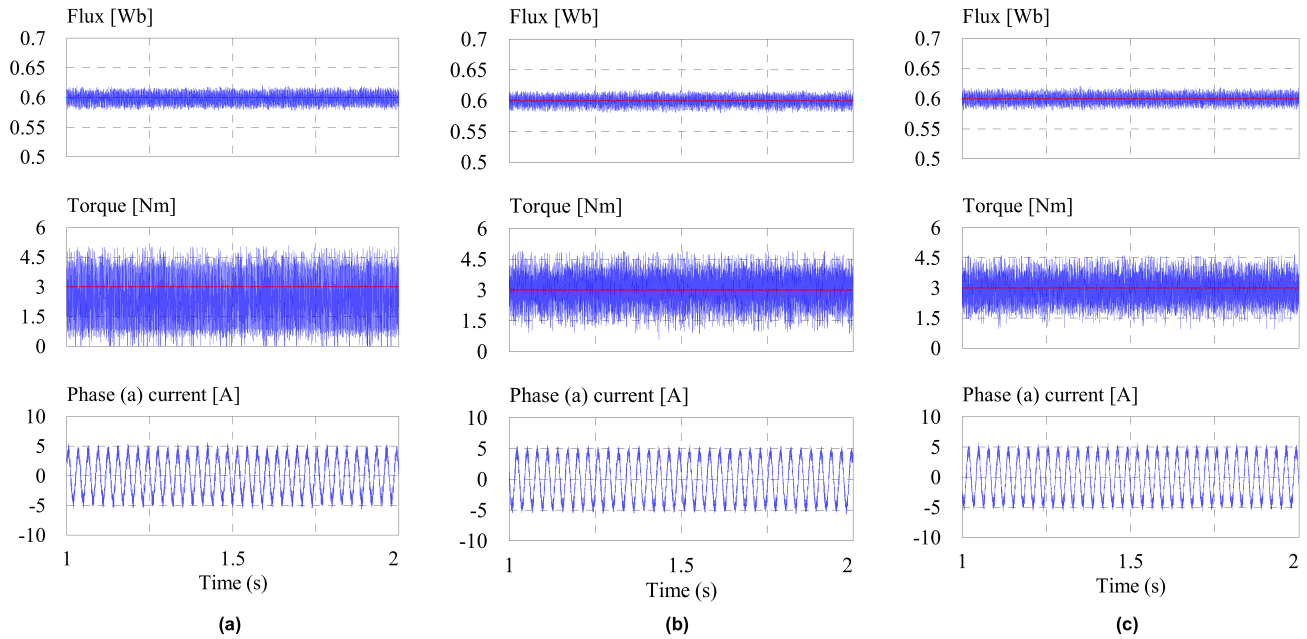
FIGURE 9. Simulation results of steady-state response of the IM at 1000 r/min, 3 Nm: (a) five-level THC; (b) conventional interleaving CSFTC; (c) proposed interleaving CSFTC; from top to bottom: flux response, torque response, stator current, and FFT analysis of the stator current (reference values: red; estimated: blue).

in high current distortion. In addition to flux-droop, a high torque ripple is noticeable. The conventional interleaving CSFTC solves the problem of flux-droop; hence, a lower THD and pure sinusoidal current waveform are achieved. However, it produces high torque and flux ripples. The proposed interleaving CSFTC attains the merits of regulating the stator flux. Moreover, the proposed method reduces the torque ripple by 36% compared to conventional interleaving CSFTC.

In addition, an FFT analysis of the stator current was carried out to verify the effectiveness of the proposed interleaving CSFTC. The proposed interleaving CSFTC achieved the lowest THD of the stator current among the other methods. The conventional interleaving CSFTC has reduced the THD of five-level THC from 25.23% to 15.62%, while the proposed interleaving CSFTC has reduced the THD to 7.05%, which is approximately 54.87%.

B. MEDIUM AND HIGH-SPEED OPERATION

Fig. 9 shows the simulation results for the five-level THC, conventional interleaving CSFTC, and proposed interleaving CSFTC based DTC methods at 1000 r/min. It is evident that the flux-droop is not critical in this speed region due to the slight effect of stator resistance. From top to bottom, the waveforms are the stator flux, torque, and stator current. The main advantage of the proposed interleaving CSFTC here is the reduction of the torque ripple compared to the five-level THC and conventional interleaving CSFTC based DTC. The torque ripple of the proposed interleaving CSFTC was reduced by 25% compared to conventional interleaving CSFTC.
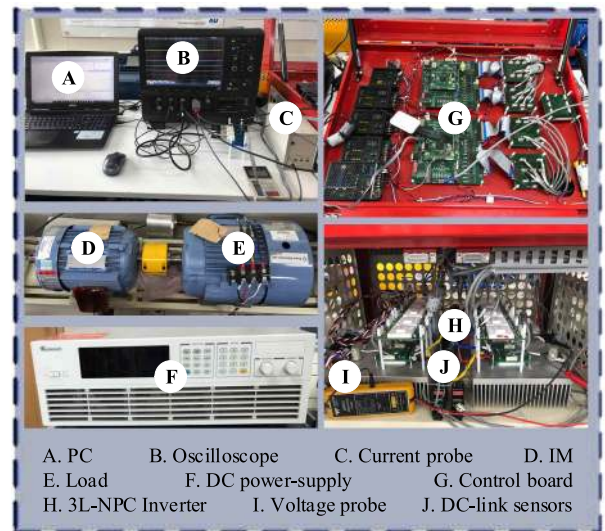

A. PC	B. Oscilloscope	C. Current probe	D. IM
E. Load	F. DC power-supply		G. Control board
H. 3L-NPC Inverter	I. Voltage probe	J. DC-link sensors	

FIGURE 10. Experimental setup.

VI. EXPERIMENTAL VALIDATION

Fig. 10 shows the experimental setup which consists of a TMS320F28335 digital signal processor (DSP) control board and 3L-NPC inverter equipped with IGBTs. A 5.5-kW mechanical load is connected to the IM and it is controlled by a Yaskawa inverter.

The discrete design of the interleaving carries CSFTC is shown in Fig. 11. This design is easily implemented by increasing the step of the carrier by 30 units per step size. The C_{p-p} value of the interleaving carriers set as 120 to allow enough amplitude of the interleaving carriers for all speed regions of the IM used in this paper. As mentioned
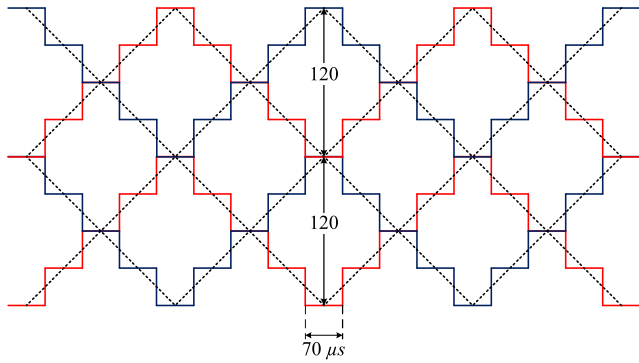
FIGURE 11. Discrete design of the interleaving CSFTC.

in Table 4, the rated speed of the IM is 1750. By using the PI gains discussed in section IV, the Tc will not exceed the C_{p-p} of the C_{upper3} and C_{upper4} for the forward operation of the IM, similarly, it will not exceed the C_{p-p} of the C_{lower3} and C_{lower4} when the IM is running in the reverse direction. The switching frequency of the interleaving carriers used in this paper is calculated by considering the sampling time which is set to 70 μs. As mentioned earlier that the step change of the interleaving carriers is by 30 units. Therefore, each step change requires 70 μs. The interleaving carriers consists of 8 steps as shown in Fig. 11. Consequently, the switching frequency of the interleaving carriers is calculated as follows:

$$f_s = (1/8 \times 70\mu s) = 1785.714 \ Hz$$

In this paper, the torque ripples are calculated based on the following equation [31]:

$$T_{e\,ripple} = \sqrt{\frac{1}{N} \sum_{i=1}^{N} (T_e(i) - T_{e\,average})^2} \qquad (13)$$

where N is the number of the samples, $T_{eaverage}$ is the average torque. For accurate $T_{e\,ripple}$ calculation, the N was set to 20,000.

A. STEADY-STATE OPERATION

The steady-state performance of three DTC methods at 50 r/min (less than 3% of the rated speed) and when a 3 Nm load torque is applied to the motor is shown in Fig. 12. In this figure, with the same sampling time of 70 μs, both the conventional and the proposed interleaving CSFTC can improve the low-speed operation by stabilizing the λ_s effectively and achieving lower THD of the i_s in comparison with the five-level THC-DTC, while the torque and flux ripples in the proposed interleaving CSFTC method are the lowest among the other three methods. In Fig. 12, the RMS value of the $T_{eripples}$ are 0.98, 1.04 and 0.68 Nm with respect to the five-level THC-DTC, the conventional interleaving CSFTC and the proposed interleaving CSFTC.

B. TRANSIENT-STATE OPERATION

In order to test the transient-state performance of the five-level THC, the conventional interleaving CSFTC and the
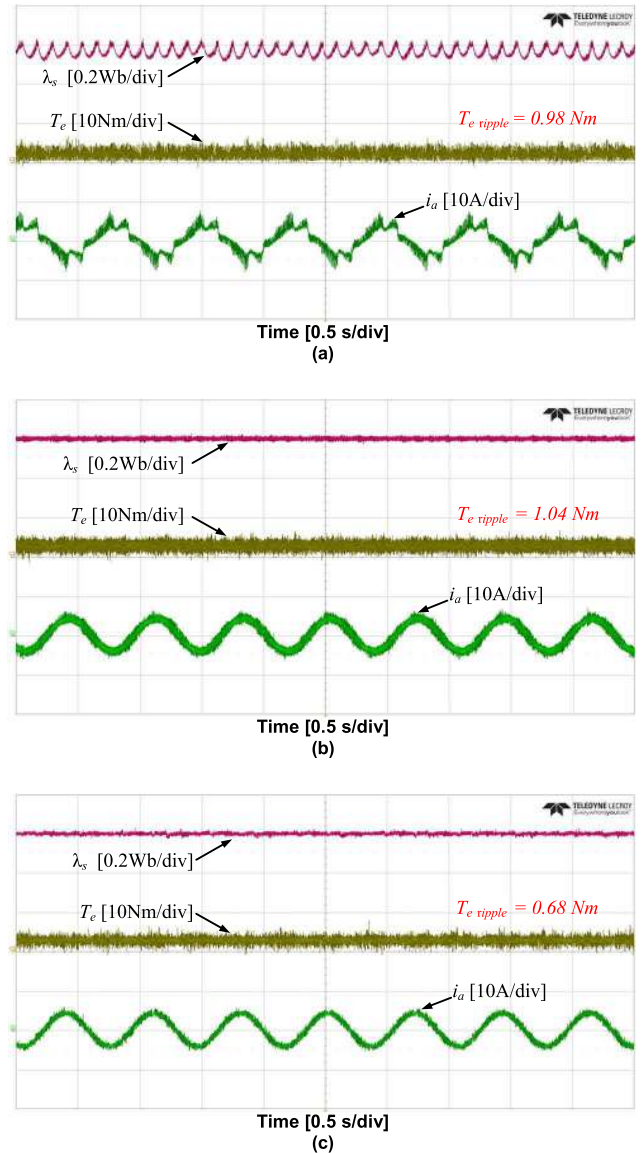

FIGURE 12. Experimental results of steady-state response of the IM at 50 r/min, 3 Nm: (a) Five-level THC; (b) conventional interleaving CSFTC; (c) proposed interleaving CSFTC; from top to bottom: flux response, torque response and stator current.

proposed interleaving CSFTC based DTC methods, when the IM rotates at 100 r/min with a load torque of 3 Nm in the steady-state, a sudden load torque of 4 Nm is applied to the IM. The experimental results are presented in Fig. 13, where it is observed that the T_e follows the T_e^* quickly and this is the main advantage of DTC. The time duration required for this process is 0.98, 1.10 and 1.00 ms for the THD-DTC, the conventional interleaving CSFTC and the proposed interleaving CSFTC, respectively. Moreover, in order to compare the dynamic response in this experiment, the zoomed torque response is also shown in Fig. 13. Although the torque response in both the conventional and the proposed CSFTC methods is almost the same, a slight difference exists in the rising time of the torque. The proposed interleaving CSFTC
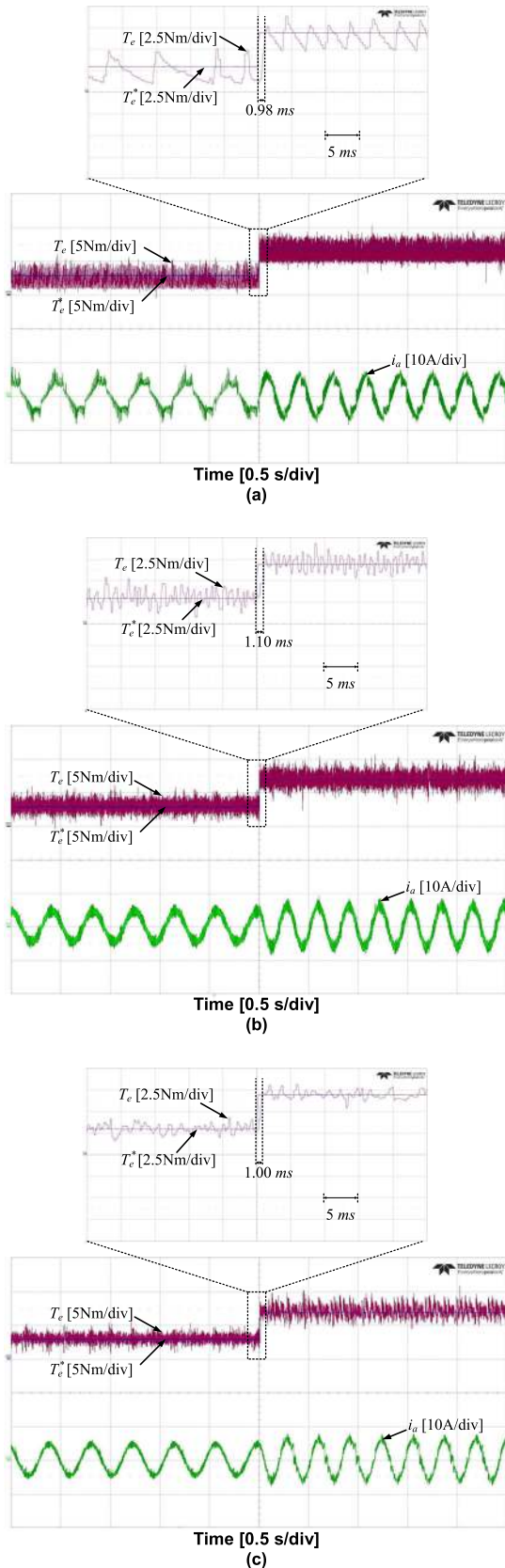
FIGURE 13. Experimental results of transient-state response of the IM at 100 r/min: (a) five-level THC; (b) conventional interleaving CSFTC; (c) proposed interleaving CSFTC; from top to bottom: estimated torque dynamic response from 3 Nm to 7 Nm and stator current.

method has the lowest $T_{e\,ripple}$ compared to the other two methods.

VII. CONCLUSION

In the high-performance IM drive applications, fast and accurate control of the torque is required. Although the conventional interleaving CSFTC provides excellent stator flux regulation at low-speed operation of the IM, it experiences high torque ripples which decrease the accuracy of the torque control and cause acoustic noises.

In this paper, interleaving CSFTC based DTC method is proposed where the duty cycles of the applied voltage vectors are shortened to maintain the merits of the conventional interleaving CSFTC in improving the low-speed operation of the IM drives and to reduce torque and flux ripples. In order to test the effectiveness of the proposed method, its performance is investigated through simulations.

The steady-state performance at various motor speeds is tested and the results indicate that the torque and flux ripples are reduced significantly in all speed ranges, compared to those of the THC-DTC and conventional interleaving CSFTC methods. In order to test the feasibility of the proposed method in practice, its performance is investigated through experiments. The steady-state operation results are in good agreement with the simulation results. In addition, the transient-state operation results reveal that the dynamic response of the proposed interleaving CSFTC is faster than that of the THC-DTC and conventional CSFTC methods.

The simulation and experimental results indicate that the proposed interleaving CSFTC improves the low-speed operation and minimizes the torque and flux ripples. Therefore, the proposed CSFTC can be considered as a good candidate for high-performance applications for IM drives.

REFERENCES

[1] I. Takahashi and T. Noguchi, "A new quick-response and high-efficiency control strategy of an induction motor," *IEEE Trans. Ind. Appl.*, vol. IA-22, no. 5, pp. 820–827, Sep. 1986.

[2] X. Sun, K. Diao, Z. Yang, G. Lei, Y. Guo, and J. Zhu, "Direct torque control based on a fast modeling method for a segmented-rotor switched reluctance motor in HEV application," *IEEE Trans. Emerg. Sel. Topics Power Electron.*, to be published.

[3] D. Casadei, F. Profumo, G. Serra, and A. Tani, "FOC and DTC: Two viable schemes for induction motors torque control," *IEEE Trans. Power Electron.*, vol. 17, no. 5, pp. 779–787, Sep. 2002.

[4] I. M. Alsofyani and N. R. N. Idris, "Simple flux regulation for improving state estimation at very low and zero speed of a speed sensorless direct torque control of an induction motor," *IEEE Trans. Power Electron.*, vol. 31, no. 4, pp. 3027–3035, Apr. 2016.

[5] I. M. Alsofyani, K. Y. Kim, S. S. Lee, and K. B. Lee, "A modified flux regulation method to minimize switching frequency and improve DTC-hysteresis-based induction machines in low-speed regions," *IEEE Trans. Emerg. Sel. Topics Power Electron.*, vol. 7, no. 4, pp. 2346–2355, Feb. 2019.

[6] C. Lascu and A. M. Trzynadlowski, "Combining the principles of sliding mode, direct torque control, and space-vector modulation in a high-performance sensorless AC drive," *IEEE Trans. Ind. Appl.*, vol. 40, no. 1, pp. 170–177, Jan./Feb. 2004.

[7] K. B. Lee and F. Blaabjerg, "An improved DTC-SVM method for sensorless matrix converter drives using an overmodulation strategy and a simple nonlinearity compensation," *IEEE Trans. Ind. Electron.*, vol. 54, no. 6, pp. 3155–3166, Dec. 2007.

[8] G. Foo, S. Sayeef, and M. F. Rahman, "Low-speed and standstill operation of a sensorless direct torque and flux controlled IPM synchronous motor drive," *IEEE Trans. Energy Convers.*, vol. 25, no. 1, pp. 25–33, Mar. 2010.

[9] J. S. Lee, C.-H. Choi, J.-K. Seok, and R. D. Lorenz, "Deadbeat-direct torque and flux control of interior permanent magnet synchronous machines with discrete time stator current and stator flux linkage observer," *IEEE Trans. Ind. Appl.*, vol. 47, no. 4, pp. 1749–1758, Jul. 2011.

[10] I. M. Alsofyani and N. R. N. Idris, "Lookup-table-based DTC of induction machines with improved flux regulation and extended Kalman filter state estimator at low-speed operation," *IEEE Trans. Ind. Informat.*, vol. 12, no. 4, pp. 1412–1425, Aug. 2016.

[11] C. Lascu, I. Boldea, and F. Blaabjerg, "A modified direct torque control for induction motor sensorless drive," *IEEE Trans. Ind. Appl.*, vol. 36, no. 1, pp. 122–130, Jan./Feb. 2000.

[12] X. Sun, Z. Shi, L. Chen, and Z. Yang, "Internal model control for a bearingless permanent magnet synchronous motor based on inverse system method," *IEEE Trans. Energy Convers.*, vol. 31, no. 4, pp. 1539–1548, Dec. 2016.

[13] X. Sun, L. Chen, Z. Yang, and H. Zhu, "Speed-sensorless vector control of a bearingless induction motor with artificial neural network inverse speed observer," *IEEE/ASME Trans. Mechatronics*, vol. 18, no. 4, pp. 1357–1366, Aug. 2013.

[14] X. Sun, C. Hu, G. Lei, Y. Guo, and J. Zhu, "State feedback control for a PM hub motor based on grey wolf optimization algorithm," *IEEE Trans. Power Electron.*, vol. 35, no. 1, pp. 1136–1146, Jan. 2020.

[15] J. Rodriguez, "State of the art of finite control set model predictive control in power electronics," *IEEE Trans. Ind. Informat.*, vol. 9, no. 2, pp. 1003–1016, May 2013.

[16] M. Habibullah and D. D.-C. Lu, "A speed-sensorless FS-PTC of induction motors using extended kalman filters," *IEEE Trans. Ind. Electron.*, vol. 62, no. 11, pp. 6765–6778, Nov. 2015.

[17] T. Geyer, G. Papafotiou, and M. Morari, "Model predictive direct torque control-Part I: Concept, algorithm, and analysis," *IEEE Trans. Ind. Electron.*, vol. 56, no. 6, pp. 1894–1905, Jun. 2009.

[18] W. Fengxiang, "An Encoderless Predictive torque control for an induction machine with a revised prediction model and EFOSMO," *IEEE Trans. Ind. Electron.*, vol. 61, no. 12, pp. 6635–6644, Dec. 2014.

[19] X. Sun, C. Hu, J. Zhu, S. Wang, W. Zhou, Z. Yang, G. Lei, K. Li, B. Zhu, and Y. Guo, "MPTC for PMSMs of EVs with multi-motor driven system considering optimal energy allocation," *IEEE Trans. Magn.*, vol. 55, no. 7, Jul. 2019, Art. no. 8104306.

[20] Y. Cho, K.-B. Lee, J.-H. Song, and Y. I. Lee, "Torque-ripple minimization and fast dynamic scheme for torque predictive control of permanent-magnet synchronous motors," *IEEE Trans. Power Electron.*, vol. 30, no. 4, pp. 2182–2190, Apr. 2015.

[21] M. H. Vafaie, B. M. Dehkordi, P. Moallem, and A. Kiyoumarsi, "Minimizing torque and flux ripples and improving dynamic response of PMSM using a voltage vector with optimal parameters," *IEEE Trans. Ind. Electron.*, vol. 63, no. 6, pp. 3876–3888, Jun. 2016.

[22] W. Chen, Y. Zhao, Z. Zhou, Y. Yan, and C. Xia, "Torque ripple reduction in three-level inverter-fed permanent magnet synchronous motor drives by duty-cycle direct torque control using an evaluation table," *J. Power Electron.*, vol. 17, no. 2, pp. 368–379, Mar. 2017.

[23] Y. Cho, Y. Bak, and K.-B. Lee, "Torque-ripple reduction and fast torque response strategy for predictive torque control of induction motors," *IEEE Trans. Power Electron.*, vol. 33, no. 3, pp. 2458–2470, Mar. 2018.

[24] N. M. Nordin, N. R. N. Idris, and N. A. Azli, "Direct torque control with 5-level cascaded H-bridge multilevel inverter for induction machines," in *Proc. 37th Annu. Conf. IEEE Ind. Electron. Soc.*, Nov. 2011, pp. 4691–4697.

[25] K.-B. Lee, J.-H. Song, I. Choy, and J.-Y. Yoo, "Improvement of low-speed operation performance of DTC for three-level inverter-fed induction motors," *IEEE Trans. Ind. Electron.*, vol. 48, no. 5, pp. 1006–1014, Oct. 2001.

[26] K.-B. Lee, J.-H. Song, I. Choy, and J.-Y. Yoo, "Torque ripple reduction in DTC of induction motor driven by three-level inverter with low switching frequency," *IEEE Trans. Power Electron.*, vol. 17, no. 2, pp. 255–264, Mar. 2002.

[27] P. Naganathan, S. Srinivas, and H. Ittamveettil, "Five-level torque controller-based DTC method for a cascaded three-level inverter fed induction motor drive," *IET Power Electron.*, vol. 10, no. 10, pp. 1223–1230, Aug. 2017.

[28] S. S. Hakami, I. M. Alsofyani, and K. B. Lee, "Improved constant switching frequency torque regulator based DTC of IM Fed by 3L-NPC inverter for wide speed region," in *Proc. IEEE Conf. Energy Convers. (CENCON)*, Oct. 2019, pp. 42–46.

[29] N. R. N. Idris and A. H. M. Yatim, "Direct torque control of induction machines with constant switching frequency and reduced torque ripple," *IEEE Trans. Ind. Electron.*, vol. 51, no. 4, pp. 758–767, Aug. 2004.

[30] N. M. Nordin, N. A. Azli, N. R. N. Idris, and N. H. Ramlan, "Constant frequency torque controller for DTC with multilevel inverter of induction machines," *Int. J. Power Electron. Drive Syst.*, vol. 7, no. 1, pp. 28–44, Mar. 2016.

[31] D. Mohan, X. Zhang, and G. Foo, "Three level inverter fed direct torque control of IPMSM with constant switching frequency and torque ripple reduction," *IEEE Trans. Ind. Electron.*, vol. 63, no. 12, pp. 7908–7918, Dec. 2016.

[32] I. M. Alsofyani, Y. Bak, and K. B. Lee, "Fast torque control and minimized sector-flux droop for constant frequency torque controller based-DTC of induction machines," *IEEE Trans. Power Electron.*, vol. 34, no. 12, pp. 12141–12153, Dec. 2019.

[33] I. M. Alsofyani and K. B. Lee, "Evaluation of direct torque control with a constant-frequency torque regulator under various discrete interleaving carriers," *Electronics*, vol. 8, no. 7, p. 820, Jul. 2019.

SAMER SALEH HAKAMI (S'19) received the B.S. degree in electrical engineering from Universiti Tun Hussein Onn Malaysia, Johor, Malaysia, in 2016. He is currently pursuing the M.S. degree in electrical and computer engineering with Ajou University, Suwon, Korea. His research interests include multilevel inverters, electric machine drives, and power conversion.

IBRAHIM MOHD ALSOFYANI (M'16) received the M.Eng. degree in electrical mechatronics and automatic control and the Ph.D. degree in electrical engineering from the Universiti Teknologi Malaysia, Johor Bahru, Malaysia, in 2011 and 2014, respectively.

From 2014 to 2016, he was a Research Associate and a Postdoctoral Fellow with the UTM-PROTON Future Drive Laboratory, Universiti Teknologi Malaysia. From 2016 to 2017, he worked as a Lecturer at the Faculty of Engineering, Lincoln University College, Malaysia. In 2017, he joined the School of Electrical and Computer Engineering, Ajou University, Suwon, South Korea, as a Research Professor, where he became an Assistant Professor, in 2018. His current research interests include electric machine drives, renewable power generations, and electric vehicle applications. He was a recipient of the Brain Korea 21 Fellowship, in 2017.

KYO-BEUM LEE (S'02–M'04–SM'10) received the B.S. and M.S. degrees in electrical and electronic engineering from Ajou University, Suwon, South Korea, in 1997 and 1999, respectively, and the Ph.D. degree in electrical engineering from Korea University, Seoul, South Korea, in 2003.

From 2003 to 2006, he was with the Institute of Energy Technology, Aalborg University, Aalborg, Denmark. From 2006 to 2007, he was with the Division of Electronics and Information Engineering, Chonbuk National University, Jeonju, South Korea. In 2007, he joined the Department of Electrical and Computer Engineering, Ajou University. His research interests include electric machine drives, renewable power generations, and electric vehicle applications. He is an Associate Editor of the IEEE TRANSACTIONS ON POWER ELECTRONICS, the IEEE TRANSACTIONS ON INDUSTRIAL ELECTRONICS, the *Journal of Power Electronics*, and the *Journal of Electrical Engineering & Technology*.

• • •